Mitochondria-targeting polydopamine-coated nanodrugs for effective photothermal- and chemo-synergistic therapies against lung cancer

Ziyu Meng[1,2], Binchao Wang[1], Yiqiang Liu[2], Yejian Wan[2], Qianshi Liu[2], Huasheng Xu[2], Renchuan Liang[2], Ying Shi[2], Peng Tu[1,*], Hong Wu[2,*] and Chuan Xu[2,*]

[1]College of Science, Gansu Agricultural University, Lanzhou 730070, China
[2]Integrative Cancer Center & Cancer Clinical Research Center, Sichuan Cancer Hospital & Institute, Sichuan Cancer Center, School of Medicine, University of Electronic Science and Technology of China, Chengdu 610047, China

*Correspondence address: Tel: +86-28-85420852, E-mail: tupeng815@163.com (P.T); wuhongzao@126.com (H.W); xuchuan100@163.com (C.X)

Abstract

Targeting mitochondria via nano platform emerged as an attractive anti-tumor pathway due to the central regulation role in cellar apoptosis and drug resistance. Here, a mitochondria-targeting nanoparticle (TOS-PDA-PEG-TPP) was designed to precisely deliver polydopamine (PDA) as the photothermal agent and alpha-tocopherol succinate (α-TOS) as the chemotherapeutic drug to the mitochondria of the tumor cells, which inhibits the tumor growth through chemo- and photothermal- synergistic therapies. TOS-PDA-PEG-TPP was constructed by coating PDA on the surface of TOS NPs self-assembled by α-TOS, followed by grafting PEG and tri-phenylphosphonium (TPP) on their surface to prolong the blood circulation time and target delivery of TOS and PDA to the mitochondria of tumor cells. *In vitro* studies showed that TOS-PDA-PEG-TPP could be efficiently internalized by tumor cells and accumulated at mitochondria, resulting in cellular apoptosis and synergistic inhibition of tumor cell proliferation. *In vivo* studies demonstrated that TOS-PDA-PEG-TPP could be efficiently localized at tumor sites and significantly restrain the tumor growth under NIR irradiation without apparent toxicity or deleterious effects. Conclusively, the combination strategy adopted for functional nanodrugs construction aimed at target-delivering therapeutic agents with different action mechanisms to the same intracellular organelles can be extended to other nanodrugs-dependent therapeutic systems.

Keywords: lung cancer; mitochondria-targeting; alpha-tocopherol succinate (α-TOS); chemo- and photothermal- synergistic therapies

Introduction

Lung cancer is a prevalent and lethal cancer worldwide. Although advances in therapeutic strategies have attracted much attention and various drugs have been developed in the past decades to prolong the survival of patients, the 5 years overall survival for advanced lung cancer patients is still < 15% [1–6]. The mitochondria of cancer cells are structurally and functionally different from their healthy counterparts, containing higher mitochondrial membrane potential, decreased oxidative phosphorylation, increased ROS production, increased mtDNA mutations, Ca^{2+} overload and failure to induce apoptosis [7–9]. Various studies have demonstrated that altered mitochondria functionality is a notable state of lung cancer and creates an exploitable vulnerability for cancer therapy [10, 11]. Hence, delivering anti-cancer drugs into mitochondria has become an attractive strategy for lung cancer therapy.
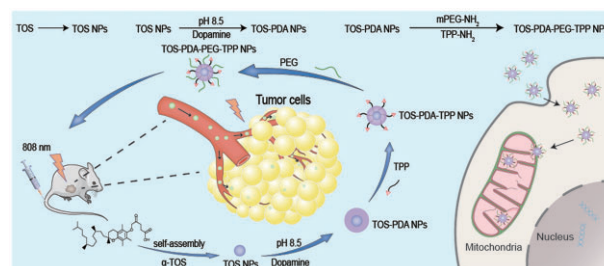
The anti-tumor effects of alpha-tocopherol succinate (α-TOS, a derivative of natural vitamin E) have been gradually discovered by targeting mitochondria to block the cell cycle, inhibit DNA synthesis and promote apoptosis or differentiation of tumor cells [12, 13]. Moreover, many studies have demonstrated that the integrated structure of α-TOS was crucial for its biological function. An urgent need to improve its anti-tumor effects was how to bring α-TOS to the mitochondrial of tumor cells in a complete form via the nano-carriers. Although mitochondria-targeting drug delivery systems have been developed in the past years, some drawbacks remain to be improved. The remarkable disadvantage is low drug-loading by carriers that could decrease treatment efficiency. To overcome the defect, we prepared carrier-free nanoparticles by α-TOS self-assemble and then modified them with functionalizing substances, making the nanoparticles with a higher drug-loading efficiency.

Nanocarriers decorated on the surface with triphenylphosphonium (TPP) are commonly used platform design in targeting the mitochondria of cells [14]. Except these, dopamine is a chemical that can self-polymerize on a variety of organic and inorganic materials by spontaneous oxidation in alkaline solutions (pH = 8.5) to form surface-adhesive polydopamine (PDA) films [15–18]. PDA shells are stable enough to reach target cells after intravenous injection. It is widely used as material surface modification [19–22]. Moreover, PDA membranes have extremely high advantages for photothermal therapy (PTT), which is a promising cancer treatment due to its low invasive burden and high spatiotemporal selectivity. In addition, PTT could rely on photothermal agents to convert the absorbed light energy into heat energy, resulting in the rise of local temperature and ultimately inducing the apoptosis of cancer cells [23–28].

In this work, we produced material for NIR-responsive PDA coating and an *in-situ* on-demand drug release system. α-TOS was used in self-assembled nanomedicines called TOS. A thin PDA film was then synthesized and exposed to the surface of the co-assembled TOS and TPP. We assumed that the TOS cycle time could be extended and the pre-leakage avoided by protecting PDA membranes. TOS passive tumor accumulation was promoted by the nanoparticles' good enhanced permeability and retention (EPR) effect [29]. Upon transport to the tumor lesions, NIR radiation might destroy PDA films, and the loaded TOS NPs were released rapidly due to the strong NIR absorption and high photothermal conversion efficiency of PDA films [30–32]. Due to their inherent hydrophobicity, TOS NPs aggregated and slowed re-entry into the bloodstream, resulting in long-term local entrapment of the drug-carrier system within the tumor microenvironment [33–37]. The photothermal effect of PDA could trigger the release of small TOS NPs, which could penetrate deeply and evenly into cancer cells [38–42]. The mitochondrial targeting function of TPP could engulf the mitochondria of tumor cells, resulting in abnormal mitochondrial membrane potential of tumor cells and further promoting the rapid apoptosis of the cancer cells [43, 44]. The enrichment of TOS NPs to tumor sites, mitochondrial targeting and time control drug-releasing realized the systematic chemical and photothermal treatment of lung cancer.

Materials and methods
Materials
D-α-TOS was purchased from Sigma-Aldrich Co., Ltd (St. Louis, MO, USA). Dopamine hydrochloride (DA·HCl) was obtained from Shanghai Aladdin Biochemical Technology Co., Ltd (Shanghai, China). (2-Aminoethyl) triphenylphosphonium bromide (TPP-NH$_2$) was bought from Accela ChemBio Co., Ltd (Shanghai, China). Tris(hydroxymethyl) aminomethane - and DMSO were purchased from Chengdu Kelong Chemical Co., Ltd (Chengdu, China). mPEG-NH$_2$ was purchased from Shanghai ToYong Bio-Tech. Inc., China.

Preparation of PDA-coated carrier-free nanodrugs
First, 50 mg α-TOS was dissolved into 2 mL DMSO solution followed by ultrasonic treatment for 10 min. Then, α-TOS solution was added dropwise into 5 mL of ultrapure water under stirring for 5 min and self-assembled into nanoparticles. Furthermore, the solution was dialyzed to remove DMSO against deionized (DI) water and then carrier-free nanoparticles (TOS NPs) solution was prepared. After that, 3 mL TOS NPs solution was mixed with 3 mL Tris-HCl solution (20 mM, pH 8.0) and then 1.2 mg DA·HCl was added to the mixture. After stirring at room temperature for 24 h,

products were collected by centrifugal ultrafiltration (MWCO 3KD) and washed with Tris-HCl solution (10 mM, pH 8.0) to remove the excess DA.

Preparation of mitochondria-targeting nanoparticles
TPP (5 mg/mL, 100 μL) and mPEG-NH$_2$ (2 mg) were added to TOS-PDA NPs (5 mL) solution for the synthesis of mitochondria-targeting nanoparticles. After stirring at room temperature for 24 h, the reaction solution was dialyzed (MWCO = 3500) against DI water to remove free reactants. Finally, we obtained the mitochondria-targeting nanoparticles (TOS-PDA-PEG-TPP NPs) solution. Similarly, the TOS-PDA-PEG NPs were prepared by adding mPEG-NH$_2$ (2 mg) to the TOS-PDA NPs solution (5 mL). After stirring at room temperature for 24 h, the reaction solution was dialyzed (MWCO = 3500) against DI water to obtain the TOS-PDA-PEG NPs solution.

Preparation of FITC-labeled nanoparticles
α-TOS and FITC were dissolved in DMSO and mixed together (ratio 10:1). The mixture was added dropwise into 5 mL of ultrapure water under stirring until the formation of nanoparticles. The solution was dialyzed to remove DMSO for 24 h against DI water and then FITC-labeled nanoparticles solution was prepared.

Characterization of nanoparticles
The hydrodynamic diameter and zeta potential of nanoparticles were measured by a Malvern Zetasizer Nano ZS90 (Worcestershire, UK). To verify the modification of PEG and TPP, FT-IR spectrums of freeze-dried nanoparticles (TOS, TOS-PDA, TOS-PDA-PEG, TOS-PDA-PEG-TPP) were recorded between 4000 and 400 cm^{-1} on an FTIR spectrometer (PerkinElmer, USA). The morphologies of the nanoparticles were observed by transmission electron microscopy (TEM).

Stability of nanoparticles
To assess the stability of nanoparticles, 500 μL nanoparticles solution was mixed with 500 μL fetal bovine serum (FBS). After 2, 6, 12, 24 and 48 h of incubation at room temperature, the mixture was photographed and measured size/zeta potential.

In vitro photothermal effects
To study the photothermal effects of the nanoparticles, 1 mL nanoparticles solution (TOS, TOS-PDA-PEG, TOS-PDA-PEG-TPP) or 1 ml water was irradiated by the 808 nm laser with the power density of 1 W/cm^2 for 5 min. To assess the photothermal constancy, the temperature curve of nanoparticles solution was measured after four-cycle on/off of NIR light. The temperature change of the solution was monitored by a thermal infrared camera and quantified by the FLIR Tools.

Cell lines and animals
Human NSCLC cell line A549 and mouse lung Lewis carcinoma (LLC) cells were purchased from the ATCC and cultured in Dulbecco's modified Eagle's medium (CA, USA) supplemented with 10% FBS (Jiangsu, China) and 100 U/ml penicillin–streptomycin. The cells were cultured at 37°C incubator with 5% CO$_2$ atmosphere. Male Balb/c mice (6–8 weeks) were purchased from Beijing Huafukang Bioscience Co. Inc and maintained in the Sichuan Cancer Institute. All animal experiments were performed in compliance with the Animal Ethics Committee of Sichuan Cancer Hospital.
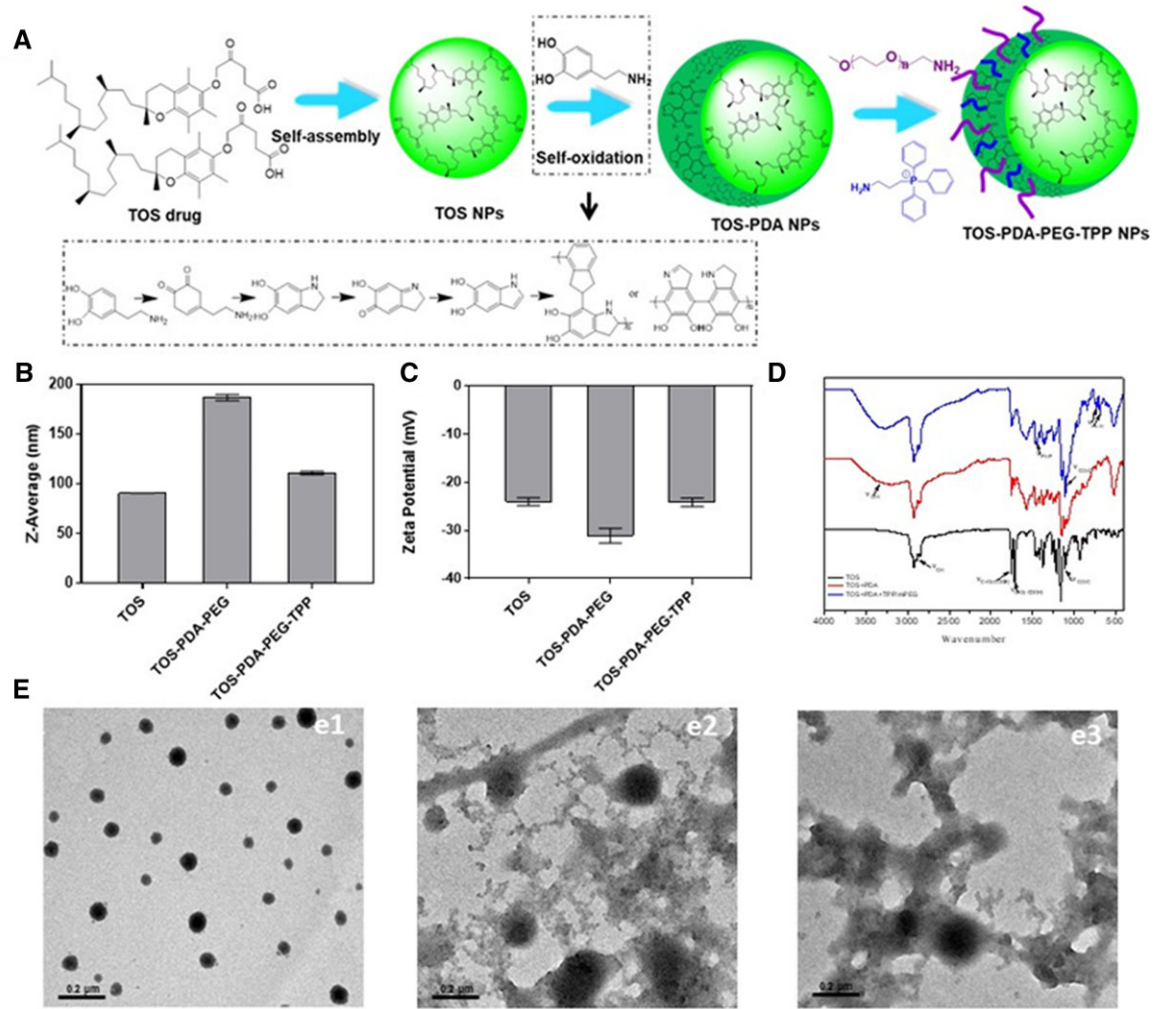
Figure 1. (**A**) The synthesis routes of mitochondria-targeting TOS-PDA-PEG-TPP NPs. (**B**) The size, (**C**) Zeta potential and (**D**) FTIR spectra of nanoparticles. (**E**) The morphologies of (e1) TOS NPs, (e2) TOS-PDA-PEG NPs, and (e3) TOS-PDA-PEG-TPP NPs.
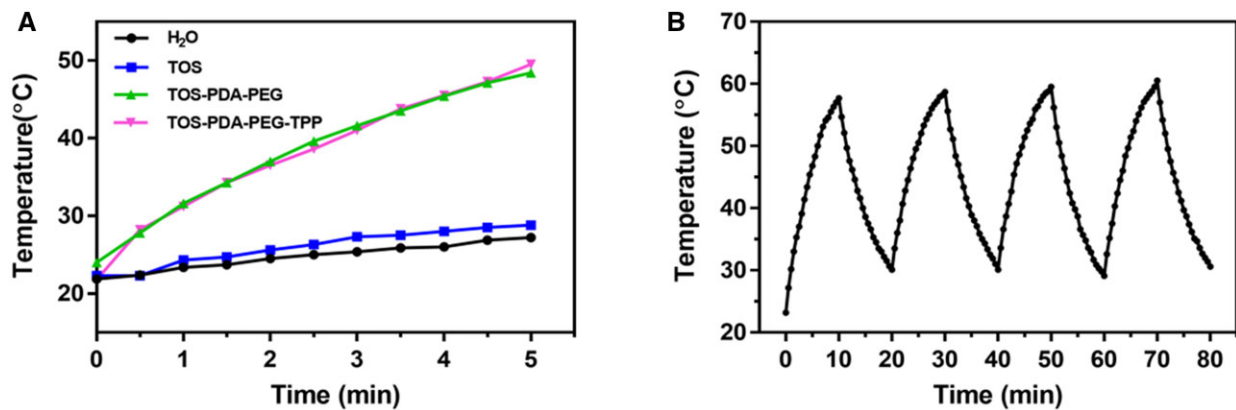

Figure 2. (**A**) Temperature changes of four groups of different materials after NIR irradiation. (**B**) Light stability of TOS-PDA-PEG-TPP for four consecutive exposures in 80 min.

Nanoparticles uptake by cancer cells

Cancer cells were seeded into six-well plates with 5×10^5 cells per well. After the cells adhered, nanoparticles were added, and the uptake of nanoparticles by cells was detected at 2 and 4 h, respectively. Confocal and flow cytometry were used to count the uptake of nanoparticles by cancer cells.

Mitochondrial targeting and co-localization of the mitochondria

The LLC cells were inoculated in six-well plates with 5×10^3 cells per well and were treated with different concentrations of nanoparticles. Mito-Tracker Red CMXROS was used according to the manufacturer's instructions (Beyotime, C1049B, China).
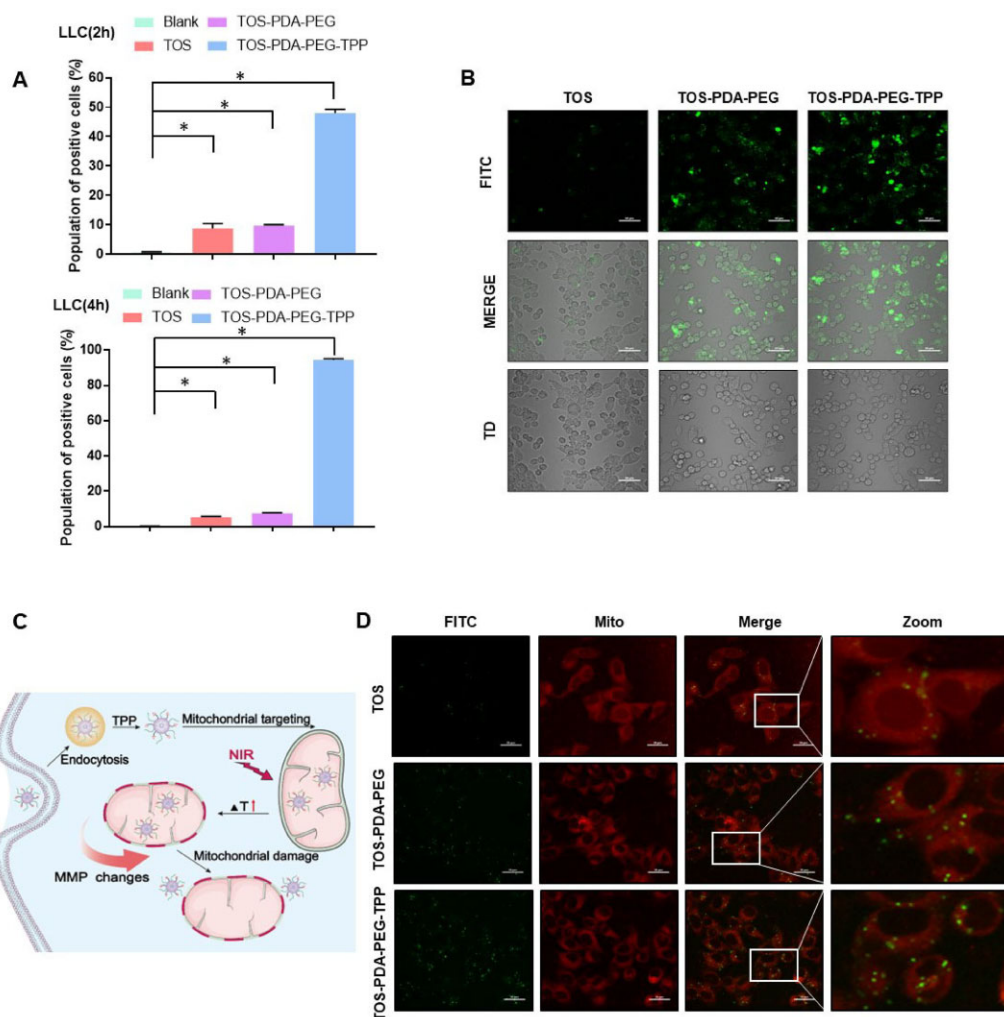
Figure 3. (**A**) Flow cytometry analysis of cellular uptake of indicated nanoparticles. (**B**) Confocal laser images of the intake of nanoparticles by LLC cells (4 h). (**C**) Schematic diagram of mitochondrial membrane potential damage caused by nanoparticles entering mitochondria. (**D**) Quantitative analysis (CLSM) of indicated nanoparticles entering mitochondria after 4 h co-culture with LLC cells.

Cell cloning experiment

Cancer cells were seeded into six-well plates at 500 cells per well with a 2 mL complete medium. After 1 week of culture, drugs were added on the 8 th, 10 th and 12 th days, respectively. On the 14th day, the cells were fixed with 4% paraformaldehyde and stained with crystal violet for 15 min to take photos and count the clones.

Cell proliferation assay

Cancer cells were cultured in 96-well plates at 4×10^3 cells per well with a 0.2 mL complete medium. Different nanoparticles were added to the complete medium and cultured with cancer cells in a 37°C for 5 days. Cell Counting Kit-8 solution (Biosharp, BS350B, Anhui, China) was diluted with the medium at a ratio of 1:10 and incubated for 2 h. Optical density was measured based on absorbance at a wavelength of 450 nm.

Mitochondrial membrane potential (ΔΨm) assay

LLC cells were treated with different nanoparticles for 24 h. The cells were washed twice with PBS, followed by JC-1 (Beyotime, C2003S, China) incubating at 37°C for 30 min in the dark. The

fluorescence intensities were analyzed using confocal with the setting of 520 nm and 590 nm.

Apoptosis assay

Apoptosis of cancer cells was detected with an Annexin V-FITC apoptosis detection kit (Beyotime, C1063, Shanghai, China) by flow cytometry according to the manufacturer's instruction. LLC cells were treated with different nanoparticles for 24 h. All cells were collected and washed twice with cold PBS, followed by incubation with 7-AAD-cy5.5 and Annexin V-FITC for 15 min at room temperature. The apoptosis was assessed by flow cytometry (BD FACSCanto II).

Western blotting

Lung cancer cells were harvested and lysed using radioimmuno-precipitation assay buffer (Thermo Fisher Scientific, 89901, MA, USA) and Phenylmethylsulfonyl Fluoride (Beyotime, ST505, Shanghai, China) mixture (100:1 ratio) on ice for 30 min. Samples were centrifuged at 15000 rpm for 20 min; supernatant was added with loading buffer and heated at 100°C for 10 min. The samples were separated by SDS-PAGE and transferred to Polyvinylidene Difluoride membranes (Millipore, IPVH00010, MA, USA). The membranes were visualized by enhanced chemiluminescence
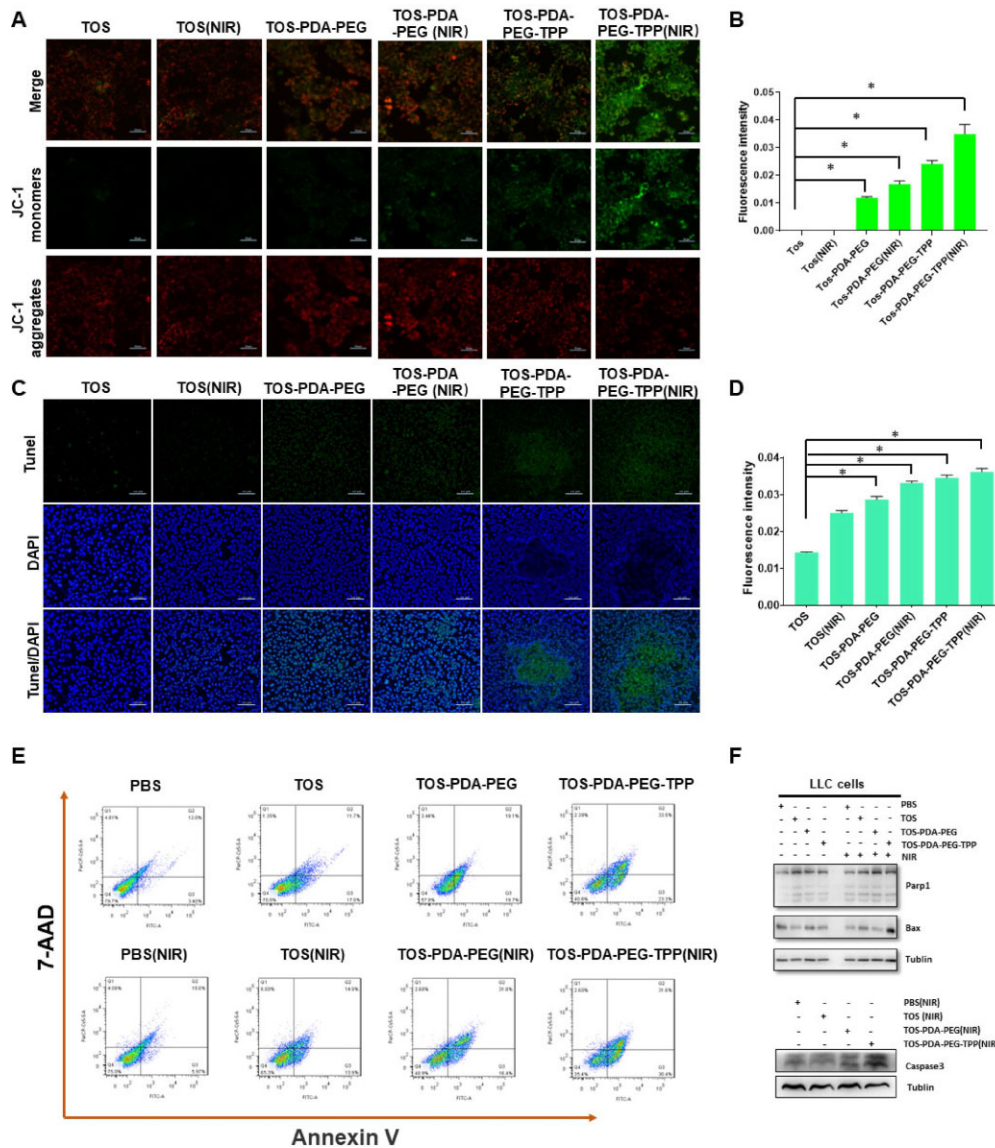
Figure 4. (**A**) Laser confocal images of indicated groups after JC-1 staining of 6 h co-culture (scale bar =50μm). (**B**) Semi-quantitative analysis of fluorescence intensity of JC-1 staining. (**C**) The confocal image of tunel after 24 h co-culture with indicated nanoparticles (scale bar = 50μm). (**D**) Semi-quantitative analysis of fluorescence intensity of tunel. (**E**) Flow cytometric analysis of annexin V and 7-AAD double staining after 24 h co-culture of indicated groups. (**F**) Protein levels of Parp1, Bax and Caspase 3 of indicated groups.

(Millipore, WBKLS0100, MA, USA). The primary antibodies were as follows: Parp1(Proteintech, #13371), Bax (CST, #14796), Caspase 3 (CST, #14220), Tublin (CST, #2148).

Fluorescence visualization

DiR-labeled NPs were used for intravital imaging and assessment of bio-distribution. Six-week-old Balb/c-Nude mice were immediately determined by fluorescent imaging after tail vein injection of DiR-labeled NPs. Time-lapse images were acquired continually within the initial 36 h after NPs injection.

In vivo anti-tumor effects

Six-week-old Balb/c mice were subcutaneously implanted with 5×10^6 LLC cells to establish a subcutaneous tumor model in mice. Ten days after inoculation, NPs were injected every other day for five times, and the NIR group was irradiated for 5 min after injection. The changes of body weight and tumor volumes were recorded. These mice were sacrificed on the 25 th day. The

lung, heart, liver, spleen, kidney and tumor of the mice were taken for physiological sections.

In vivo photothermal effect

Lung cancer mice model was established as mentioned above. NPs were injected by the tail vein. After 2 h, the mice were irradiated by 808 nm near-infrared light. The temperature changes of the tumors were observed by a photothermal imaging instrument.

HE staining

Paraffin sections were stained with hematoxylin and eosin (HE) staining for morphometric analysis. Paraffin sections were dewaxed with different concentrations of xylene and alcohol. The slices were stained with hematoxylin staining solution (Harris) for 3 min and then differentiated with 0.8% hydrochloric acid. These slices were stained with eosin stain for 20 s, rinsed with water for 5 min and transparently sealed.
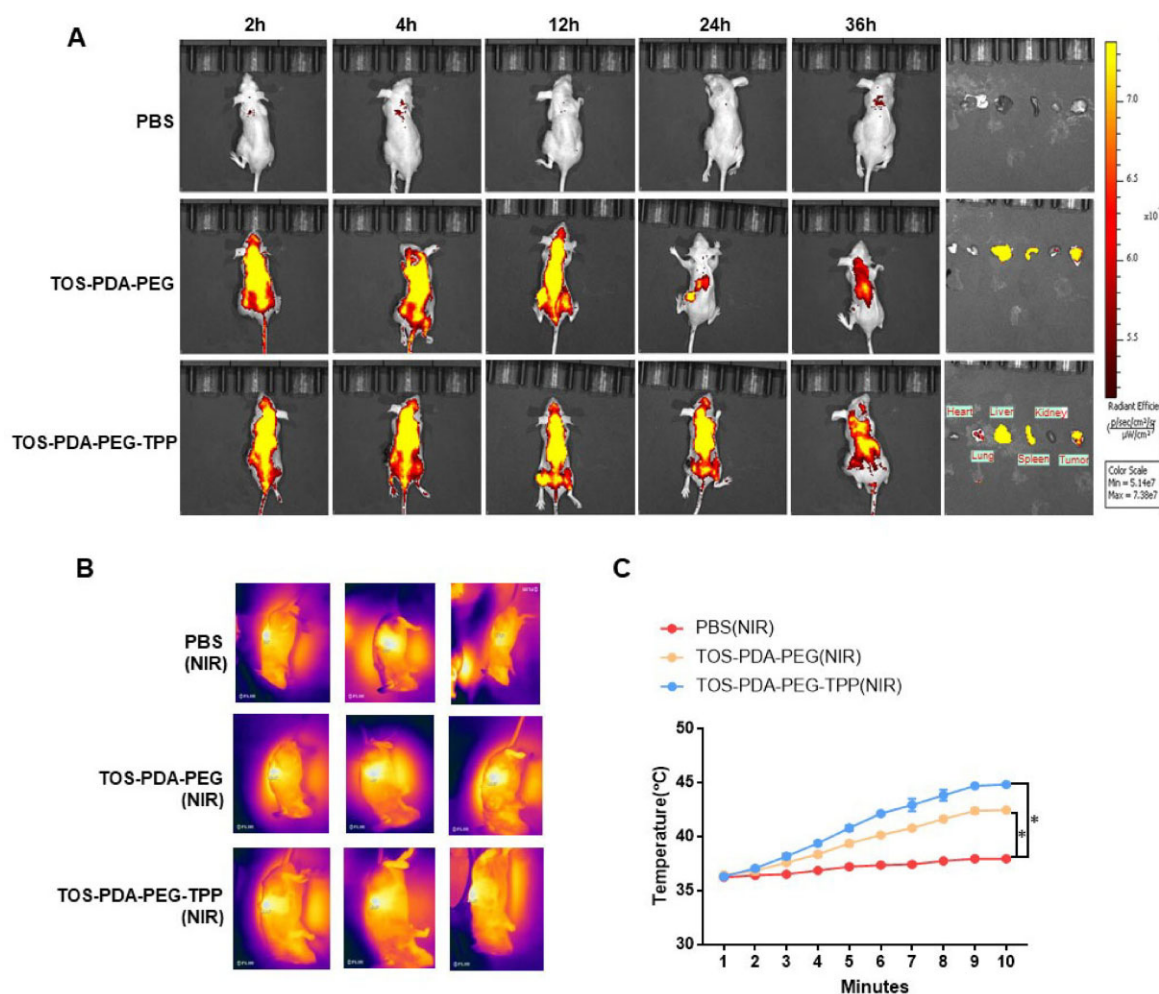
Figure 5. (**A**) Distribution of drugs in mice at different time points (2 h, 4 h, 12 h, 24 h, 36 h) after tail vein injection. (**B**) The temperature changes of mice after different drugs were injected into the tail vein and irradiated by NIR. (**C**) Temperature changes at the tumor site over 10 min.

Immunohistochemistry analysis

Immunohistochemical staining was performed on tissue slides using the streptavidin–biotin–peroxidase complex method. The procedure of antigen extraction was to place the sample in the antigen extraction solution containing 10 mM sodium citrate buffer and heat it in a pressure pot. Ki-67 antibody (CST, 1:200) and CD31 antibody (CST, 1:100) were used to detect. Slides were counterstained with hematoxylin.

Statistical analysis

Statistical analysis was performed with GraphPad Prism 7.0 (CA, USA). Statistical significance was determined by one-way ANOVA or unpaired Student's T-test. All data used in this study satisfied the assumptions of the statistical tests. All quantitative data were shown as the mean ± S.D. P values were indicated. $P < 0.05$ was considered statistically significant.

Results and discussion

Preparation and characterizations of self-assembled nanoparticles

To synthesize the nanoparticles, α-TOS was dissolved in DMSO solution to prepare nanoparticles (TOS NPs) by self-assemble. Then, the TOS NPs solution was mixed with Tris-HCl solution, and DA·HCl was added to form PDA-coated TOS-PDA NPs by self-oxidation polymerization. Mitochondrially targeted nanoparticles (TOS-PDA-PEG-TPP NPs) were finally obtained by adding TPP and mPEG-NH$_2$ into the TOS-PDA NPs solution. The mitochondrial targeting TOS NPs synthesis pathway is shown in Fig. 1A. We observed that the particle sizes of nanoparticles were < 200 nm by particle size potentiometer (Fig. 1B). Compared with TOS NPs, the widths of TOS-PDA-PEG and TOS-PDA-PEG-TPP nanoparticles were slightly increased, which was an essential characterization of the successful modification of TOS NPs. It is well known that the particle size of the nano drug carrier affects its cumulative efficiency and endocytosis efficiency at the tumor sites. The nanocarrier with a particle size < 200 nm is more likely to reach the tumor site through the EPR effect. The zeta potentials of TOS, TOS-PDA-PEG and TOS-PDA-PEG-TPP nanoparticles were all distributed between –20 and –35 mV (Fig. 1C). The absorption peaks of functional groups were also apparent in their spectra (Fig. 1D). The absorption peak of TOS can be observed by UV-visible absorption spectroscopy (Supplementary Fig. S1). The peak of TOS-PDA-PEG and TOS-PDA-PEG-TPP have no apparent deviation, and the introduction of PDA and TPP has slight effect on the energy absorption of nanoparticles. TEM was used to observe the morphology of TOS, TOS-PDA-PEG and TOS-PDA-PEG-TPP. As shown in Fig. 1E, TOS formed spherical nanoparticles. When coated with PDA, TOS-PDA-PEG and TOS-PDA-PEG-TPP showed apparent
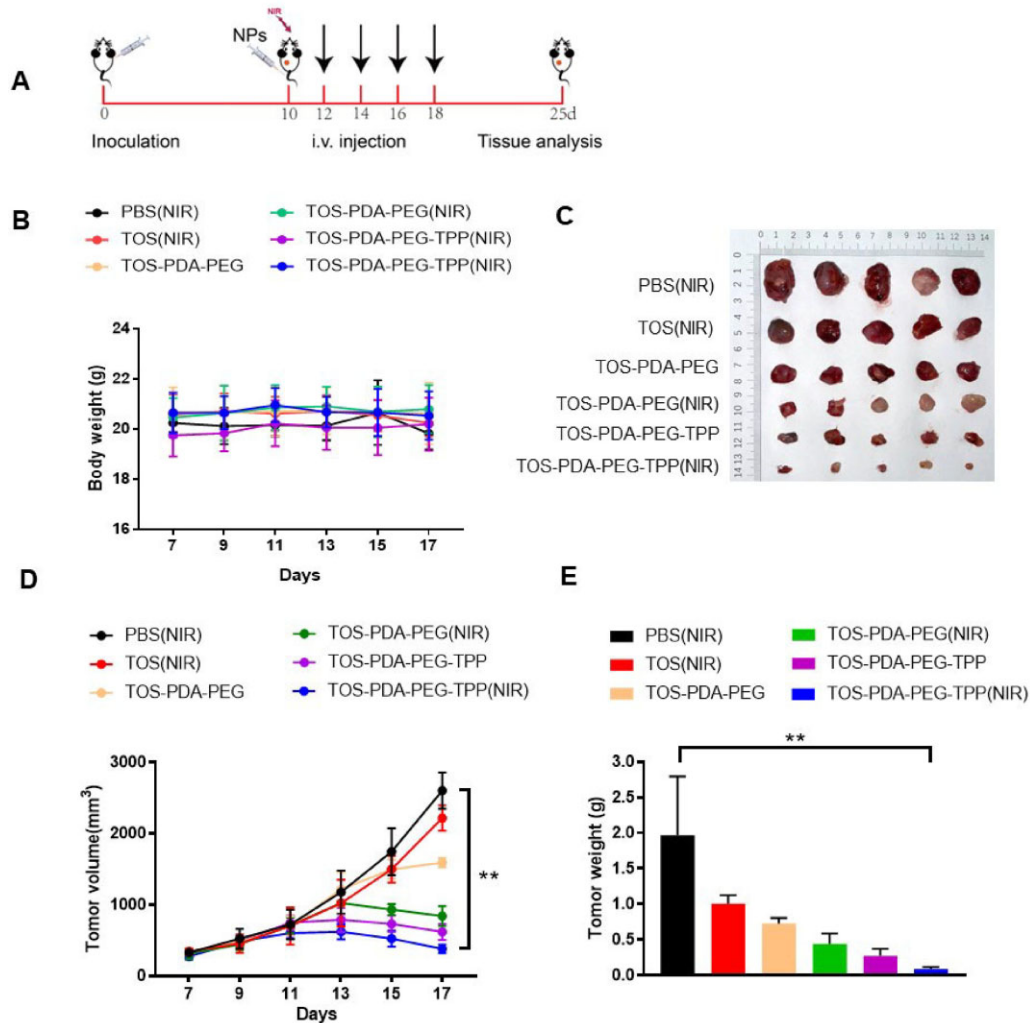
Figure 6. (**A**) Schematic diagram of tumor inoculation and administration in mice. (**B**) Body weight changes of mice in indicated groups after drug injection. (**C**) Tumor images of indicated groups of mice after treatment. (**D**) Changes in tumor volume in six groups during treatment. (**E**) Statistical map of tumor weight of six groups of mice after treatment.

membrane structure and uniform particle size distribution. Compared with single TOS, the particle size increased slightly, indicating that PDA was successfully coated on the surface of TOS. The results were consistent with the previous characterization data.

As shown in Fig. 2A and B, compared with the control group H$_2$O and TOS, the temperatures of TOS-PDA-PEG and TOS-PDA-PEG-TPP continue to rise, under the continuous irradiation with a near-infrared light for 5 min. The temperature of TOS-PDA-PEG-TPP has reached 50°C, which provides the necessary conditions for subsequent anti-tumor treatment. The strength of nanoparticles is a critical evaluation index of drug delivery *in vivo*, which plays a decisive role in the later anti-tumor effect. In this study, the nanoparticles were co-cultured with 5% serum to simulate the *in vivo* environment, and the changes in particle size and potential with time were observed (Supplementary Fig. S2). At the initial stage of co-culture, the particle size decreased slightly. With the increase of culture time, the particle size and the potential increased slightly. However, the particle size was stable, and the particle size was < 200 nm, indicating that the nanoparticles had good stability in the serum solution. The above results showed that the constructed TOS-PDA-PEG-TPP in this study had good stability and had the potential to prolong the circulation

time in the blood, thereby increasing the amount of TOS-PDA-PEG-TPP reaching the tumor site.

In vitro cellular uptake

To address whether the nanoparticles could be engulfed by tumor cells, we did flow cytometry and confocal laser scanning microscopy. Flow cytometry showed that both LLC and A549 cells could absorb FITC-labeled nanoparticles after co-culture for 2 h or 4 h, respectively (Fig. 3A, Supplementary Fig. S3A). Tumor cells showed more vital ability for TOS-PDA-PEG-TPP NPs uptake. Similar results were observed in LLC cells by confocal microscopy (Fig. 3B). Since TPP has been reported to have mitochondrial-targeting properties, we loaded TPP into the engineered nanoparticles to guide the drugs to mitochondria. To demonstrate whether TPP decorated NPs could realize mitochondrial targeting, we did confocal microscopy by staining the cells with mitotracker and FITC-labeled nanoparticles treatment. Results showed that TOS-PDA-PEG-TPP nanoparticles increased mitochondrial accumulation compared to TOS NPs and TOS-PDA-PEG NPs (Fig. 3C and D). These results indicate that the designed nanoparticles can be well engulfed by tumor cells and realize mitochondrial-targeting ability effectively.
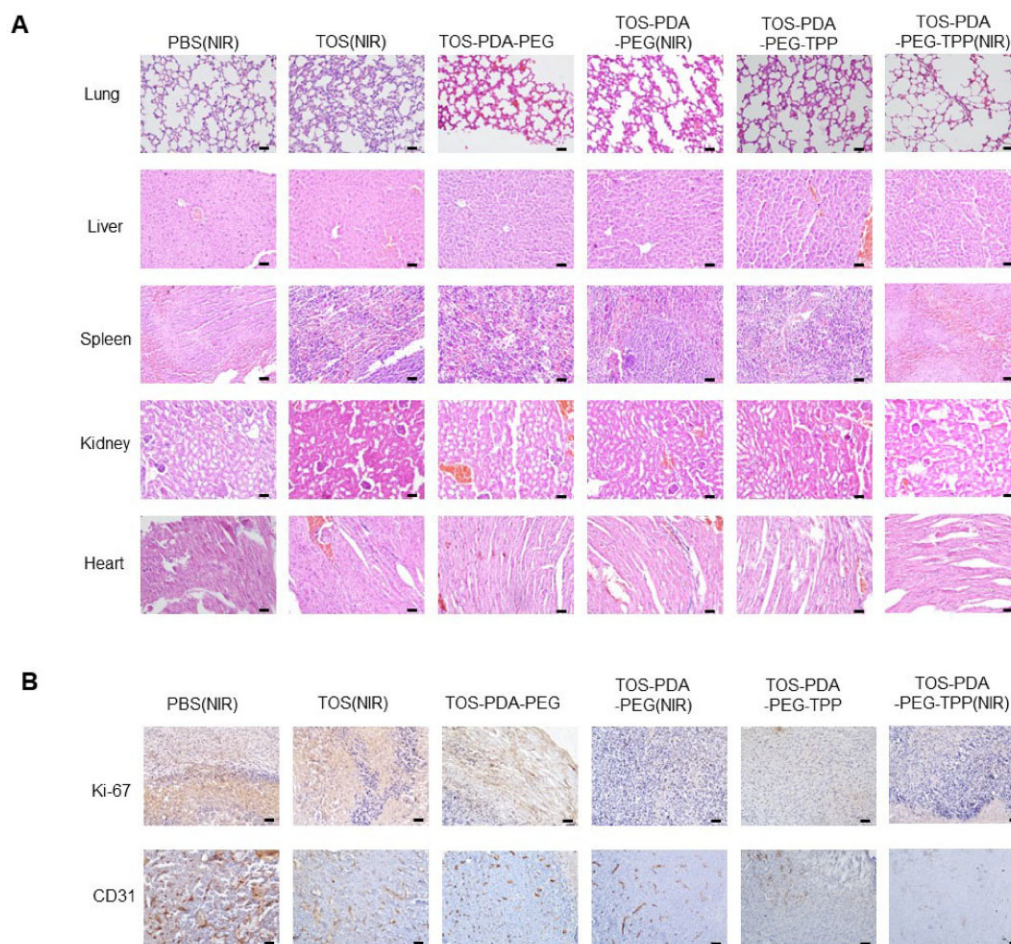
Figure 7. (**A**) HE staining (lung, liver, spleen, kidney, heart and tumor) of mice treated with indicated drugs (scale bar = 100 μm). (**B**) Immunohistochemical staining (Ki-67, CD31) of indicated mice treated with different drugs (scale bar =100 μm).

In vitro anti-tumor effects of nanoparticles

We conducted several assays to explore the anti-tumor effect of these nanoparticles. First of all, we detect the changes in mitochondrial membrane potential. Results showed that the membrane potential decreased significantly upon TOS-PDA-PEG-TPP NPs treatment and NIR irradiation (Fig. 4A and B). This may be result by the enhanced mitochondrial targeting ability of TOS-PDA-PEG-TPP NPs. It is well known that the decrease in mitochondrial membrane potential is a hallmark event in the early stages of apoptosis. We used confocal microscopy and flow cytometry to detect the early apoptosis of cancer cells treated with different nanoparticles. Confocal microscopy showed that TOS-PDA-PEG-TPP NPs combined with NIR treatment increased the apoptosis of cancer cells significantly (Fig. 4C and D). Western blot showed that the expressions of Parp1, Bax and Caspase 3 were increased dramatically in the TOS-PDA-PEG-TPP(NIR) group. However, NIR treatment alone did not induce apoptosis (Fig. 4E and F). We also carried out a cloning formation assay, and results showed that the TOS-PDA-PEG-TPP group could exert a better anti-cancer effect than TOS alone (Supplementary Fig. S4A). These results showed that the TOS-PDA-PEG-TPP (NIR) composite treatment could enhance the mitochondrial targeting impact of nanoparticles and promote cell apoptosis by changing the mitochondrial membrane potential.

In vivo anti-tumor effects of different nanoparticles

To explore the tumor-targeting effect of nanoparticles, we injected them through the tail vein in a subcutaneous xenograft nude mouse model. Then, the *in vivo* distribution of nanoparticles was detected in the next 36 h using *in vivo* imaging technology. Results indicated that TOS-PDA-PEG-TPP was distributed throughout the body within the first 2 h after intravenous injection and then accumulated in the tumor sites effectively at 36 h (Fig. 5A). This result indicated that the nanoparticles loaded with TPP had accurate tumor targeting and could effectively transport the drug to the tumor sites of mice. In photothermal imaging, TOS-PDA-PEG-TPP reached 45°C in 10 min after near-infrared light irradiation. Results showed that the maximum temperature of drugs without TPP reached 42°C, resulting in corresponding lethal effects on tumors (Fig. 5B and C). It indicated that *in vitro* near-infrared irradiation combined with *in vivo* drug treatment ruptured the PDA coating membrane of nanoparticles and released drugs against tumor cells.

To further explore the anti-tumor effect and side effects of nanoparticles *in vivo*, we established a subcutaneous tumor transplantation model in mice and explored the combined effect of nanocomposites and PTT. The mice were divided into six groups: PBS(NIR), TOS(NIR), TOS-PDA-PEG, TOS-PDA-PEG(NIR), TOS-PDA-PEG-TPP, TOS-PDA-PEG-TPP(NIR). As shown in Fig. 6A,

we performed treatment experiments on the 10th day after inoculating subcutaneous xenografts. Nanoparticles were injected intravenously every 2 days, and NIR treatment was performed 2 h post-injection. The results showed no significant change in the body weight of the mice (Fig. 6B), TOS-PDA-PEG-TPP NPs combined with NIR treatment had the most excellent anti-tumor effects, and the subcutaneously transplanted tumor was significantly decreased (Fig. 6C–E).

We further performed HE staining and the results showed no obvious damage to essential organs such as the heart, liver, spleen, etc., suggesting that the nanoparticles did not have noticeable side effects on animals (Fig. 7A). In addition, we performed immunohistochemical staining on tumor tissues to examine the expression levels of CD31 and Ki-67 in tumors. The results suggested that the expression levels of CD31 and Ki-67 in the TOS-PDA-PEG-TPP (NIR) group were significantly decreased, which indicated that nanoparticles could reduce substantially the angiogenesis and proliferation of subcutaneous xenograft tumors and had an excellent therapeutic effect (Fig. 7B). In conclusion, our experiments demonstrate that the designed nanoparticles have an anti-tumor effect in mice.

Conclusion

In this study, we used a novel near-infrared laser-induced nanoparticle delivery system to prolong the blood circulation time of TOS NPs. Moreover, TPP was introduced as mitochondria-targeting drug to realize the subcellular localization to enhance the anti-tumor effect of TOS NPs. It not only solved the shortcomings of easy dissolution and poor photostability of TOS but also proved that the composite nanoparticles could accelerate the apoptosis of tumor cells by changing the mitochondrial membrane potential *in vitro* and *in vivo*. In addition, *in vivo* experiments showed that NIR-irradiated nanoparticles could rapidly rise tumor temperature, have excellent EPR effect and effectively reduce nanoparticle toxicity *in vivo*. In conclusion, the results have opened up a new route for the self-assembly of carrier-free nanoparticles based on PTT.

Supplementary data

Supplementary data are available at *REGBIO* online.

Acknowledgements

We thank all the members of Prof. Xu's Laboratory from Sichuan Cancer Hospital.

Author contributions

Z.M. performed the experiments. Z.M., B.W., Y.L. and H.W. wrote and reviewed the original draft. H.W., Y.S., Q.L., H.X., R.L. and Y.W. provided suggestions and technical support for the project. H.W., P.T. and C.X. processed data curation, methodology, project administration and supervised and validated the project. All authors discussed the results and commented on the manuscript.

References

1. Chen F, An P, Liu L, Gao Z, Li Y, Zhang Y, Sun B, Zhou J. A polydopamine-gated biodegradable cascade nanoreactor for pH-triggered and photothermal-enhanced tumor-specific nanocatalytic therapy. *Nanoscale* **2021**;13:15677–88.
2. Chen Q, Zhang L, Li L, Tan M, Liu W, Liu S, Xie Z, Zhang W, Wang Z, Cao Y, Shang T, Ran H. Cancer cell membrane-coated nanoparticles for bimodal imaging-guided photothermal therapy and docetaxel-enhanced immunotherapy against cancer. *J Nanobiotechnology* **2021**;19:449.
3. Dai G, Chu JCH, Chan CKW, Choi CHJ, Ng DKP. Reactive oxygen species-responsive polydopamine nanoparticles for targeted and synergistic chemo and photodynamic anticancer therapy. *Nanoscale* **2021**;13:15899–915.
4. Fan B, Fan Q, Hu L, Cui M, Wang X, Ma H, Wei Q. Polydopamine-PEG-folic acid conjugate film engineered TiO$_2$ nanotube arrays for photoelectrochemical sensing of folate binding protein. *ACS Appl Mater Interfaces* **2020**;12:1877–84.
5. Fang Y, Xing C, Zhan S, Zhao M, Li M, Liu H, Wang C. Multifunctional magnetic-fluorescent nanoparticle: fabrication, bioimaging, and potential antibacterial applications. *ACS Biomater Sci Eng* **2019**;5:6779–93.
6. Boix-Montesinos P, Soriano-Teruel PM, Armiñán A, Orzáez M, Vicent MJ. The past, present, and future of breast cancer models for nanomedicine development. *Adv Drug Deliv Rev* **2021**;173:306–30.
7. Couvreur P. Nanoparticles in drug delivery: past, present and future. *Adv Drug Deliv Rev* **2013**;65:21–3.
8. Hacioglu C. Capsaicin inhibits cell proliferation by enhancing oxidative stress and apoptosis through SIRT1/NOX4 signaling pathways in HepG2 and HL-7702 cells. *J Biochem Mol Toxicol* **2021**;e22974.
9. Han L, Liu M, Yan B, Li Y, Lan J, Shi L, Ran R. Polydopamine/polystyrene nanocomposite double-layer strain sensor hydrogel with mechanical, self-healing, adhesive and conductive properties. *Mater Sci Eng C Mater Biol Appl* **2020**;109:110567.
10. Li Y, Hu P, Wang XL, Hou X, Liu FZ, Jiang XH. Integrin αvβ 3-targeted polydopamine-coated gold nanostars for photothermal ablation therapy of hepatocellular carcinoma. *Regen Biomater* **2021**;8:rbab046.
11. Jiang L, Li L, He X, Yi Q, He B, Cao J, Pan W, Gu Z. Overcoming drug-resistant lung cancer by paclitaxel loaded dual-functional liposomes with mitochondria targeting and pH-response. *Biomater* **2015**;52:126–39.
12. Mei H, Li J, Cai SS, Zhang XQ, Shi WQ, Zhu H, Cao J, Bin H. Mitochondria-acting carrier-free nanoplatform self-assembled by a-tocopheryl succinate carrying cisplatin for combinational tumor therapy. *Regen Biomater* **2021**;8:1–11.
13. Aracely AM, Julio RL. The role of alpha tocopheryl succinate (α-TOS) as a potential anticancer agent. *Nutr Cancer* **2014**;66:167–76.
14. Edgar PH, Patricia GG, Jaime GM, Matias L, Araceli D, Carmen E. New injectable two-step forming hydrogel for delivery of bioactive substances in tissue regeneration. *Regen Biomater* **2019**;6:149–162.
15. Lei Z, Ding L, Yao C, Mo F, Li C, Huang Y, Yin X, Li M, Liu J, Zhang Y, Ling C, Wang Y. Highly efficient tumor-targeting nanoprobe

with a novel cell membrane permeability mechanism. *Adv Mater* **2019**;31:e1807456.

16. Han RX, Liu QY, Lu Y, Peng JR, Meng P, Wang GH, Chen W, Xiao Y, Yang CL, Qian ZY. Tumor microenvironment-responsive Ag2S-PAsp(DOX)-cRGD nanoparticles-mediated photochemotherapy enhances the immune response to tumor therapy. *Biomater* **2022**;281:121328.

17. Hu H, Liu X, Hong J, Ye NB, Xiao C, Wang JH, Li ZF, Xu DF. Mesoporous polydopamine-based multifunctional nanoparticles for enhanced cancer phototherapy. *J Colloid Interface Sci* **2022**;612:246–60.

18. Li M, Sun X, Ning Z, Wei W, Yang Y, Jia H, Liu W. NIR-activated polydopamine-coated carrier-free "nanobomb" for in situ on-demand drug release. *Adv Sci (Weinh)* **2018**;5:1800155.

19. Li X, Guo D, Hu Y, Chen Y. Oxidative stress and inflammation are associated with coexistent severe multivessel coronary artery stenosis and right carotid artery severe stenosis in elderly patients. *Oxid Med Cell Longev* **2021**;2021:2976447.

20. Kim HS, Seo M, Park TE, Lee DY. A novel therapeutic strategy of multimodal nanoconjugates for state-of-the-art brain tumor phototherapy. *J Nanobiotechnol* **2022**;20:14.

21. Wei XJ, Chen S, Xie T, Chen HC, Jin X, Yang JM, Sahar S, Huang HL, Zhu SJ, Liu NB, Yu CJ, Zhu P, Wang W, Zhang W. An MMP-degradable and conductive hydrogel to stabilize HIF-1alpha for recovering cardiac functions. *Theranostics* **2022**;12:127–42.

22. Xie L, Li J, Wang GH, Sang W, Xu MZ, Li WX, Yan J, Zhang B, Li Z, Zhao Q, Yuan Z, Fan QL, Dai YL. Phototheranostic metal-phenolic networks with antiexosomal PD-L1 enhanced ferroptosis for synergistic immunotherapy. *J Am Chem Soc* **2022**;144:787–97.

23. Xiong Y, Wang Z, Wang Q, Deng Q, Chen J, Wei J, Yang X, Yang X, Li Z. Tumor-specific activatable biopolymer nanoparticles stabilized by hydroxyethyl starch prodrug for self-amplified cooperative cancer therapy. *Theranostics* **2022**;12:944–62.

24. Yang HY, Zhou JY, Duan ZJ, Lu B, Deng B, Xu WL. Preparation of structural color on cotton fabric with high color fastness through multiple hydrogen bonds between polyphenol hydroxyl and lactam. *ACS Appl Mater Interfaces* **2022**;14:3244–54.

25. Yang X, Wang D, Zhu J, Xue L, Ou C, Wang W, Lu M, Song X, Dong X. Functional black phosphorus nanosheets for mitochondria-targeting photothermal/photodynamic synergistic cancer therapy. *Chem Sci* **2019**;10:3779–85.

26. Li S, Zhang Y, Liu X, Tian Y, Cheng Y, Tang LG, Lin HR. Smart NIR-II croconaine dye-peptide for enhanced photo-sonotheranostics of hepatocellular carcinoma. *Theranostics* **2022**;12:76–86.

27. Liu J-S, Peng S-J, Li G-F, Zhao Y-X, Meng X-Y, Yu X-R, Li Z-H, Chen J-M. Polydopamine nanoparticles for deep brain ablation via near-Infrared irradiation. *ACS Biomater Sci Eng* **2020**;6:664–72.

28. Liu Q, Yang T, Ye Y, Chen P, Ren XN, Rao A, Wan Y, Wang B, Luo Z. A highly sensitive label-free electrochemical immunosensor based on an aligned GaN nanowires array/polydopamine heterointerface modified with Au nanoparticles. *J Mater Chem B* **2019**;7:1442–9.

29. Lu Q, Qi S, Li P, Yang L, Yang S, Wang Y, Cheng Y, Song Y, Wang S, Tan F, Li N. Photothermally activatable PDA immune nanomedicine combined with PD-L1 checkpoint blockade for antimetastatic cancer photoimmunotherapy. *J Mater Chem B* **2019**;7:2499–511.

30. Chen M, Zhang Y, Zhang Y, Rizvi SFA, Fu GQ, Liu XY, Zhang HX. A pH-targeted and NIR-responsive NaCl-nanocarrier for photothermal therapy and ion-interference therapy. *Nanomedicine* **2022**;39:102460.

31. Ma L, Diao L, Peng ZF, Jia Y, Xie HM, Li BS, Ma JT, Zhang M, Cheng LF, Ding DW, Zhang XN, Chen HB, Mo FF, Jiang HL, Xu GQ, Meng FH, Zhong ZY, Liu M. Immunotherapy and prevention of cancer by nanovaccines loaded with whole-cell components of tumor tissues or cells. *Adv Mater* **2021**;33:2104849.

32. Ma L, Huang S, He S, Wang Z, Cheng Z. Polydopamine-coated downconversion nanoparticle as an efficient dual-modal near-infrared-II fluorescence and photoacoustic contrast agent for non-invasive visualization of gastrointestinal tract in vivo. *Biosens Bioelectron* **2020**;151:112000.

33. Ma T, Zhao Y, Ruan K, Liu X, Zhang J, Guo Y, Yang X, Kong J, Gu J. Highly thermal conductivities, excellent mechanical robustness and flexibility, and outstanding thermal stabilities of aramid nanofiber composite papers with Nacre-Mimetic layered structures. *ACS Appl Mater Interfaces* **2020**;12:1677–86.

34. Maruthapand M, Jacob N, Ehud B. Antibacterial activity against methicillin-resistant *Staphylococcus aureus* of colloidal polydopamine prepared by carbon dot stimulated polymerization of dopamine. *Nanomaterials* **2019**;9:1731.

35. Fu LY, Hua XW, Jiang XY, Shi JJ. Multistage systemic and cytosolic protein delivery for effective cancer treatment. *Nano Lett* **2022**;22:111–8.

36. Luo R, Ou CQ, Li XC, Wang YF, Du W, Liang GL, Gong CY. An acidity-initiated self-assembly/disassembly nanoprobe to switch on fluorescence for tumor-targeted near-infrared imaging. *Nano Lett* **2022**;22:151–6.

37. Tran HA, Tran PA. Immobilization-enhanced eradication of bacterial biofilms and in situ antimicrobial coating of implant material surface – an in vitro study. *Int J Nanomedicine* **2019**;14:9351–60.

38. Yang Z, Zhang L, Wei JL, Li RQ, Xu Q, Hu H, Xu ZS, Ren JH, Wong CY. Tumor acidity-activatable photothermal/fenton nanoagent for synergistic therapy. *J Colloid Interface Sci* **2022**;612:355–66.

39. Yu QH, Zhang CM, Jiang ZW, Qin SY, Zhang AQ. Mussel-inspired adhesive polydopamine-functionalized hyaluronic acid hydrogel with potential bacterial inhibition. *Glob Chall* **2020**;4:1900068.

40. Zhang TX, Hou XX, Kong Y, Yang F, Yue YX, Shah MR, Li HB, Huang F, Liu JF, Guo DS. A hypoxia-responsive supramolecular formulation for imaging-guided photothermal therapy. *Theranostics* **2022**;12:396–409.

41. Mallick A, More P, Sougata G, Chippalkatti R, Chopade BA, Lahiri M, Basu S. Dual drug conjugated nanoparticle for simultaneous targeting of mitochondria and nucleus in cancer cells. *ACS Appl Mater Interfaces* **2015**;7:7584–98.

42. Min H, Wang J, Qi YQ, Zhang YL, Han XX, Xu Y, Xu JC, Li Y, Chen L, Cheng K, Liu GN, Yang N, Li YY, Nie GJ. Biomimetic metal-organic framework nanoparticles for cooperative combination of antiangiogenesis and photodynamic therapy for enhanced efficacy. *Adv Mater* **2019**;31:1808200–11.

43. Shao D-D, Yang W-J, Xiao H-F, Wang Z-Y, Zhou C, Cao X-L, Sun S-P. Self-cleaning nanofiltration membranes by coordinated regulation of carbon quantum dots and polydopamine. *ACS Appl Mater Interfaces* **2020**;12:580–90.

44. Taylor AT, Iraganje E, Lai EPC. A method for the separation of TiO$_2$ nanoparticles from water through encapsulation with lecithin liposomes followed by adsorption onto poly(L-lysine) coated glass surfaces. *Colloids Surf B Biointerfaces* **2020**;187:110732.